Les Houches Winter School: Physics and Astrophysics of Planetary Systems
Editors : will be set by the publisher
EAS Publications Series, Vol. ?, 2008

EVAPORATION OF EXTRASOLAR PLANETS

David Ehrenreich[1]

Abstract. Atomic hydrogen escaping from the extrasolar giant planet HD 209458b provides the largest observational signature ever detected for an extrasolar planet atmosphere. In fact, the upper atmosphere of this planet is evaporating. Observational evidences and interpretations coming from various models are reviewed. Implications for exoplanetology are discussed.

1 Introduction

Extrasolar planets are now commonly found around main sequence stars, usually by measuring the variations of the stellar velocity projected on the line of sight. If the inclination of the planetary system is close to 90°, the planet is seen from Earth passing in front of its host star: this transiting event is the current best tool used to characterize extrasolar planets. The transit of HD 209458b, producing a $\sim 1\%$ dip in the stellar light curve, has permitted to confirm the gaseous nature of extrasolar giant planets (Charbonneau et al. 2000; Henry et al. 2000). Using transmission spectroscopy, it was further possible to probe the composition and structure of the planet atmosphere.

Transmission spectroscopy consists in measuring the depth of the transit light curve – which is related to the planetary radius – as a function of wavelength (see the contribution of Marley in this volume). Atmospheric sodium is for instance detected as a supplementary absorption of $\sim 10^{-4}$ in the Na I D lines at 589 nm (Charbonneau et al. 2002). Since the absorption is located in the core of the lines, it appears stronger ($\lesssim 10^{-3}$) at a better spectral resolution, thus probing higher altitudes in the planet atmosphere (Sing et al. 2008; Snellen et al. 2008), typically $\sim 1\,000$ km above the optically thick radius r_p resulting from Rayleigh scattering by molecular hydrogen (Lecavelier des Etangs et al. 2008). Yet, it remains a tenuous signature in the visible.

[1] Laboratoire d'astrophysique de Grenoble
Université Joseph Fourier and CNRS (UMR 5571)
BP 53 38041 Grenoble cedex 9, France
david.ehrenreich@obs.ujf-grenoble.fr

DOI: (will be inserted later)

On the other hand, intriguing strong absorptions were observed during the planetary transit in some atomic lines located in the ultraviolet part of the spectrum: the Lyman α (Lyα) line of neutral hydrogen (H I) at 121.6 nm yields a dimming of 5 to 15% depending on the spectral resolution (Vidal-Madjar et al. 2003, 2004, 2008; Ben-Jaffel 2007; Ehrenreich et al. 2008) and lines of atomic oxygen (O I) around 130.5 nm and singly ionized carbon (C II) close to 133.5 nm show a dip between 7 and 13% (Vidal-Madjar et al. 2004).

In fact, these absorptions are larger than the signature of the planet itself during the transit. Hence, they must originate in the planet upper atmosphere at the level of the Roche lobe. Consequently, this gas must be escaping the planet gravity: HD 209458b is evaporating. After giving some keys to the understanding of the escape process (§2), I will review the observational results (§3) and their possible interpretations (§4). Finally, I will discuss the implications and prospects of evaporation in the frame of comparative exoplanetology (§5).

2 Exosphere and atmospheric escape: some definitions

All the notions addressed in this chapter are developed by Chamberlain & Hunten (1987), where the reader is referred for more details.

2.1 Collisionless atmospheres

A planetary atmosphere can be roughly split in two parts: the bottom part is the homosphere, where atmospheric constituants are mixed by various processes (convection in the troposphere, eddy diffusion, molecular diffusion, collisions, etc.) resulting in a more-or-less uniform composition with a mean molar mass μ. On the contrary, in the upper heterosphere, the density is weak enough so that molecules and atoms are stratified by the planet gravity as a function of their molar masses. The uppermost fringes of the heterosphere constitute the exosphere.[1]

An exosphere is collisionless: the base of the exosphere, dubbed exobase or critical level, is defined as the altitude r_c where the atmospheric scale height H equals the mean free path l of gas atoms (usually, hydrogen atoms). Exospheres of close-in giant exoplanets extend up to their Roche radii r_R (Lecavelier des Etangs et al. 2004). In other words,

$$\int_{r_c}^{r_R} n(r) Q \mathrm{d}r \approx n(r_c) Q H = \frac{H}{l(r_c)} = 1, \tag{2.1}$$

where r is the distance to the planet centre, n is the number density (in g cm^{-3}), Q is the collision cross section (cm^2), and $H = \mathrm{R}T_c/\mu g_p$ with R (erg K^{-1} mol^{-1}) the universal gas constant, T_c (K) the exospheric temperature, and μ (g mol^{-1}) the mean molar mass of the atmosphere. The scale height can be considered constant

[1] Exo ($\acute{\epsilon}\xi o$) means 'outside', just as in 'exoplanet': a planet that lies outside of our solar system. The exosphere is the boundary between an atmosphere and the space outside.

across the exosphere. An important point concerning giant exoplanet atmospheres is that $T_c \gg T_{\rm eff}$.[2]

2.2 Escape processes

Being a boundary layer between a relatively dense gas envelope and space vacuum, the exosphere is where atmospheric mass loss processes, or escape processes, take place. The simplest, yet usually not very efficient, escape mechanism is the thermal escape (Jeans 1925). It assumes that particles in the exosphere have a Maxwell-Boltzmann velocity distribution with a most probable velocity u depending on the temperature at the exobase as $u = (2{\rm R}T_c/\mu)^{1/2}$. Only particles in the tail of the velocity distribution, with speeds exceeding the escape velocity $v_{\rm esc} = (2{\rm G}m_p/r_p)^{1/2}$ where G is the gravitational constant, can escape. The Jeans escape flux in $\rm s^{-1}$ is

$$F_J = \frac{n(r_c)u}{2\pi^{1/2}}(1+\lambda_c)\exp{(-\lambda_c)}, \tag{2.2}$$

with the parameter λ_c expressing the absolute value of the gravitational potential energy at the exobase in units of ${\rm R}T_c$,

$$\lambda_c = \frac{{\rm G}m_p\mu}{{\rm R}T_c r_c} = \left(\frac{v_{\rm esc}}{u}\right)^2 = \frac{r_c}{H}. \tag{2.3}$$

At high λ_c, Jeans escape is a *diffusion-limited* process because the flux of escaping particles must be balanced by the flux of particles reaching the exobase from below. It generally gives a lower limit to the actual escape flux and remains valid providing $\lambda_c \gg 2$, i.e., the speed of the expanding isothermal atmosphere is much less that the sound speed at the exobase (Walker 1982).

The Jeans escape flux severely underestimate the measured escape rate of planets in the solar system. Their atmospheric mass loss is in fact controlled by 'non-thermal' processes, a review of which can be found in Hunten (1982). One mechanism known in the solar system and proposed to occur at HD 209458b is charge-exchange reactions between the neutral exosphere and stellar wind protons (Holmström et al. 2008; see §4), which can produce energetic neutral atoms with high velocities, from the reaction ${\rm H} + {\rm H}^{+*} \rightarrow {\rm H}^{+} + {\rm H}^{*}$.

Non-thermal escape processes are likely at play in the exospheres of extrasolar planets. However, a major difference with the solar system is that $\sim 30\%$ of extrasolar planets has semi-major axis below 0.1 astronomical units (AU). For these planets, the star is a tremendous source of energetic X and extreme ultraviolet (EUV) photons that are able to heat the upper atmospheric layers (the thermosphere) to $\sim 10^4$ K (Lammer et al. 2003). Ballester, Sing & Herbert (2007) provided an observational evidence of such high temperature by detecting the signature of excited hydrogen atoms H I ($n = 2$), which population peaks around

[2]For instance, on Jupiter $T_c \lesssim 1\,000$ K, much higher than the planet effective temperature (Smith & Hunten 1990).

10^4 K. Under these extreme heating conditions, λ_c reaches small values and the expanding atmosphere experiences a 'blow off' (Hunten 1982) where its bulk velocity becomes supersonic. At this point, the best description of atmospheric escape is not that of Jeans, nor the limit to the escape flux is the transport to the exobase; the description is rather hydrodynamic and the energetic input to the upper atmosphere represents the bottleneck to the escape flux.

Furthermore, close-in giant extrasolar planets are deeply embedded in the gravitational well of their host stars, so that their extended atmospheres are especially sensitive to tides. Lecavelier des Etangs et al. (2004) showed that tidal forces enhance the escape rate of a hot Jupiter and pull the exobase level up to the Roche limit, where the atmosphere is free to escape the planet gravity, leading to a *geometrical blow-off* (see also Gu, Lin & Bodenheimer 2003).

2.3 Roche lobe

The gravitational potential of a rotating circularized binary system, such as a star-planet system, expresses (Hameury 2000)

$$\phi = -\frac{\mathrm{G}m_p}{|x - r_p|} - \frac{\mathrm{G}m_\star}{|x - r_\star|} - \frac{1}{2}|\omega \times x|^2, \tag{2.4}$$

where x is the distance from the centre of mass and ω is the system angular speed. The five points where the condition $\nabla\phi = 0$ is satisfied are the Lagrangian points ($\mathrm{L}_1, \ldots, \mathrm{L}_5$), all located in the orbital plane. The first 3 Lagrangian points are aligned with the centres of the planet and the star. Figure 1 represents the equipotential lines around the extrasolar planet HD 209458b with the L_1 and L_2 points. The Roche limit is the equipotential passing through L_1; it delimits the lobe of the planet gravitational influence. The Roche lobe is elongated toward the star and in the opposite direction and has therefore a radial ($r_\parallel$) and transverse ($r_\perp$) radii, with $r_\parallel > r_\perp$. During a transit, the cross section of the Roche lobe is $4\pi r_\perp^2$, conveniently approximated by the equivalent Roche radius r_R, defined so that $4/3\pi r_R^3$ is equal to the volume within the Roche lobe (Paczyński 1971). This radius can be estimated to better than 1% by (Eggleton 1983)

$$r_{\mathrm{Roche}} = \frac{0.49q^{2/3}}{0.6q^{2/3} + \ln\left(1 + q^{1/3}\right)}, \quad 0 < q < \infty, \tag{2.5}$$

where $q = m_p/m_\star$ and the separation of the two body centres in unity.

3 Observations of the exospheres of extrasolar planets

3.1 Detection of the escaping exosphere of HD 209458b from resolved data

The transit of HD 209458b was originally observed by Vidal-Madjar et al. (2003) with the Space Telescope Imaging Spectrograph (STIS; Woodgate et al. 1998) on board the *Hubble Space Telescope* (*HST*) to search for H I in the planet atmosphere.

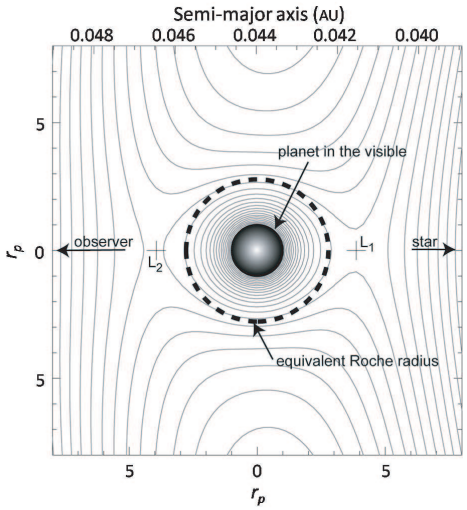

Fig. 1. Gravitational equipotentials around HD 209458b. The Roche equivalent radius is delimited by the thick dashed circle. The actual Roche limit is elongated toward the star and in the opposite direction. During a transit, the observer see the small section of the Roche lobe, which size is slightly overestimated by the equivalent Roche radius.

Since H I is the lightest possible component of the planet, it could be detected high in the atmosphere, resulting in a large absorption signal. Indeed, a surprisingly strong absorption of $(15 \pm 4)\%$ was measured in the Lyα stellar emission line at 121.6 nm, monitored during 3 transits and shown in Fig. 2. The corresponding light curve is plotted in the upper panel of Fig. 3. A difficulty of the analysis was to cautiously remove the contribution of the varying geocoronal Lyα emission from the measurement.

The observation can be interpreted as the signature of an extended and escaping exosphere of H I. The authors argumentation is two-fold: (i) a Roche lobe of radius $r_\perp \approx r_R = 2.8\ r_p$ filled with H I would produce a dip of $\sim 11\%$ in the transit light curve. The value measured is larger, some hydrogen must be observed beyond the Roche lobe. Moreover, (ii) the resolution of the spectrograph allowed the authors to report an absorption spanning from -130 to +100 km s^{-1} with respect to the centre of the Lyα stellar line. These velocities are above the escape velocity of the planet (43 km s^{-1}) and, therefore, hydrogen must again be escaping the planet. These observations allowed to constrain the escape rate $\dot{m}$ of the planet atmosphere to $\sim 10^{10}$ g s^{-1} (see §4).

Ben-Jaffel (2007) measured an absorption of $(8.9 \pm 2.1)\%$, lower than the value given by Vidal-Madjar et al. (2003). However, this difference is due to the choice of a larger bandpass over the Lyα line (see Fig. 2) and the fact that the absorption takes place at the core of the line (see Vidal-Madjar et al. 2008 for details).

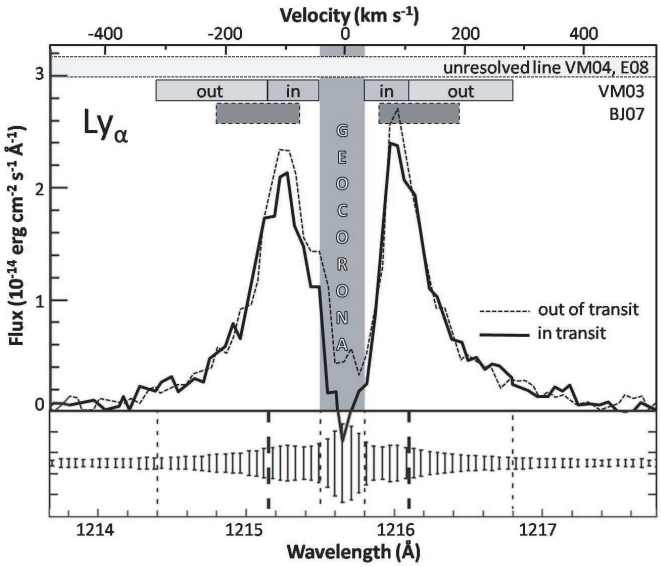

Fig. 2. The Lyα emission line of star HD 209458. The continuum is a double peaked emission originating from the stellar chromosphere. The central part of the line is absorbed by interstellar H I and deuterium in the line of sight. It is also the place where the geocoronal emission contaminates the spectrum. The 2003 STIS medium-resolution spectrum is shown outside and inside the transit (upper panel) with the 1-σ error bars (bottom panel). Bandpasses of the different Lyα measurements are indicated, from top to bottom: Vidal-Madjar et al. (2004) and Ehrenreich et al. (2008) determined the absorption by integrating over the whole unresolved Lyα line in 2004 STIS low-resolution and 2005 ACS low-resolution data, respectively; Vidal-Madjar et al. (2003) normalized the flux in the 'in' domain by that in the 'out' bands to correct for variations of the stellar Lyα flux (see Vidal-Madjar 1975 for a study of solar Lyα variations); Ben-Jaffel (2007) integrated the flux of the 2003 STIS data in a broader domain than Vidal-Madjar et al. (2003).

3.2 Constraints on the evaporation of HD 209458b from unresolved data

The detection of HD 209458b extended exosphere was first confirmed by Vidal-Madjar et al. (2004) with low-resolution STIS spectra gathered during 4 transits of the planet. A low-resolution grism was employed to probe a large spectral domain in the ultraviolet (from 120 to 170 nm) and test whether other atomic elements could be seen in the exosphere. Light curves were calculated by integrating over several unresolved atomic lines. Besides H I Lyα, oxygen (O I), carbon (C II), and various lines of silicium, suflur, and nitrogen were tested. The 3 latter elements did not show any significant absorption during the transit, whilst a $(5.3 \pm 1.9)\%$ dip was observed in the Lyα line (light curve in the middle panel of Fig. 3). Because

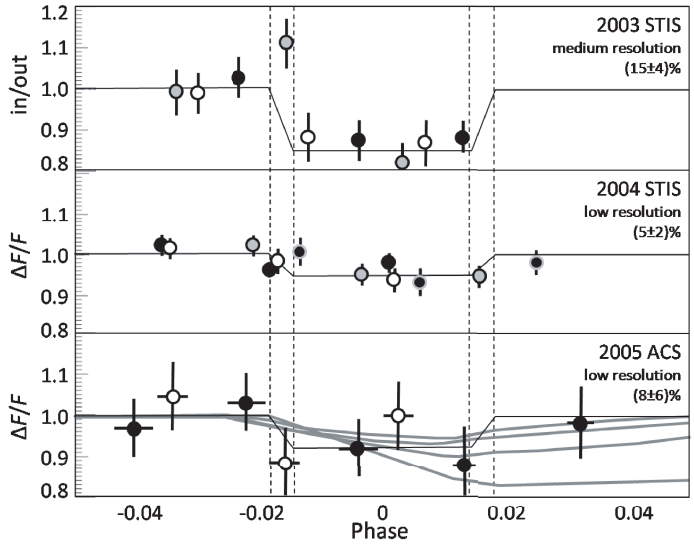

Fig. 3. Ultraviolet transit light curves of HD 209458b at Lyα, for three different data sets. Different colours correspond to different *HST* visits. Trapezoidal fits to the light curves are included, whose depths have been determined by (from top to bottom) Vidal-Madjar et al. (2003, 2004) and Ehrenreich et al. (2008). The bins used by these authors are represented in Fig. 2. Theoretical light curves resulting from the passage of a hydrogen comet-like tail trailing the planet are figured in the bottom panel, for different $\dot{m}$.

this value is obtained by integrating over the entire unresolved Lyα line, it is compatible with the $(15 \pm 4)\%$ previously measured over $\sim 1/3$ of the line.

Large absorptions of $(12.8 \pm 4.5)\%$ and $(7.5 \pm 3.6)\%$ during the transit were also determined from fits to the light curve of the stellar flux integrated over neutral oxygen (O I, O I*, and O I**) and ionized carbon (C II and C II*) lines, respectively.

This brought new constraints on the escape mechanism. In fact, atoms heavier than hydrogen must be carried to high altitudes by the flow of escaping hydrogen atoms with a velocity $u \sim 10$ km s^{-1} (at 10^4 K), close to the speed of sound: the escape is hydrodynamic, i.e., the escape rate is enhanced by the upward bulk velocity at the top of the atmosphere, as in a 'blow-off' scenario (see §2.2). In addition, the observational signatures of O I*, O I**, and C II* show that collisions are necessarily happening at these high altitudes in order to populate these excited levels. This implies Roche lobe densities of $n \sim 10^6$ cm^{-3}. It is remarkable that these simple observational constraints provide an estimate of $\dot{m} = 4\pi r_R^2 u \mu n / \mathrm{N_A} \sim 10^{10}$ g s^{-1}, with μ the molar mass of H and $\mathrm{N_A}$ the Avogadro number, which is compatible with previous, independent estimates (see also Vidal-Madjar 2005).

3.3 Are there other cases of evaporation?

The atmospheric evaporation phenomenon was first observed in 2003 when the number of transiting planets around bright stars ($V \lesssim 10$) was minute. The situation drastically changed in 2004, when several 'bright' transits were spotted, in particular, HD 149026b ($V = 8.15$; Sato et al. 2005) and HD 189733b ($V = 7.67$; Bouchy et al. 2005). Unfortunately, another drastic event later this year was STIS stopping operations because of a power supply failure. The Advanced Camera for Surveys (ACS; Ford et al. 2003) on board *HST* was then used as a back-up solution for programs aimed at obtaining new data on these two planets in addition to HD 209458b.

A prism can be inserted before the ACS detector to perform slitless spectroscopy at Lyα, with a spectral resolution close to STIS low-resolution mode but – as data revealed – a lesser sensitivity. Transit light curves at Lyα can presently be obtained for the three above-mentioned planets. Archived ACS data of HD 149026b[3] seem not precise enough, though, to detect any potential extended exosphere for this planet enriched in heavy element; this is mainly due to the weak Lyα emission of the transited G star.

Additional observations of HD 209458b were obtained in 2005; their analysis yielded a new measurement of the absorption of the exospheric hydrogen during the transit: $(8.0 \pm 5.7)\%$ (Ehrenreich et al. 2008; light curve in the bottom panel of Fig. 3). This result, although weakly significant, remains compatible with previous detections, and acts as a benchmark for the study of a more promising target: HD 189733b. ACS data for this planet orbiting a K star with a strong Lyα emission are being obtained at the time of writing.

4 Models of atmospheric evaporation

4.1 Interpreting the observations

Models of extended exospheres have early been crafted by observers to justify the search for large spectroscopic signatures (Rauer et al. 2000; Moutou et al. 2001) and, later, to provide an interpretation of the 15% absorption in the Lyα stellar line during the transit (Vidal-Madjar et al. 2003). These last authors used a particle simulation in which the escape rate $\dot{m}$ is a free parameter (Vidal-Madjar & Lecavelier des Etangs 2004). Hydrogen atoms with velocities $\sim v_{\rm esc}$ are blown by the planet at $\dot{m}$ and sensitive to the known and wavelength-dependent stellar radiation pressure, that accelerates them to the high velocities observed. The radiation pressure on the moving planet carves the cloud of escaping atoms as a comet-like tail, trailing the planet. Schneiter et al. (2007) employed a three-dimensional hydrodynamical simulation to treat the interactions between the stellar wind blown at a fixed rate and an isotropic wind of H atoms ejected by the planet for various

[3]Program #10718, principal investigator: J.A. Valenti.

values of $\dot{m}$. Their simulations also show a cometary structure for the cloud of escaping material.

Escaping atoms are also submitted to the planetary and stellar gravity. Lecavelier des Etangs et al. (2004) considered the effect of tidal forces, and found that tides shape the exosphere into an elongated 'rugby ball'[4]; they calculated that the escape rate is enhanced toward the star and in the opposite direction. The neutral H atoms are ionized by EUV photons on a short time scale ($\sim$ 6 h). Thus, the size of the hydrogen tail should depend on the stellar EUV flux.

The models then simulate the transit of the planet and its hydrogen cloud, and convolve the resulting light curves with a synthetic Lyα stellar profile. They are able to reproduce the observed emission profile and the absorption measured during the transit assuming $\dot{m} \sim 10^9$ to 10^{10} g s^{-1}. They also predict an asymmetric shape for the transit curve, because of the passage of the comet-like tail following the planet. Current observations do not have the precision nor the appropriate phase coverage of the orbit to evidence this structure (Ehrenreich et al. 2008).

Holmström et al. (2008) proposed that the high velocities of the reported absorption cannot be explained by the radiation pressure, but rather by the recombination of solar wind protons in the planet exosphere *via* charge-exchange reactions (see §2.2). The cloud of neutral hydrogen produced by their particle simulation is able to reproduce the observed Lyα profile during the transit, although it does so at the unlikely condition that the radiation pressure is lower than the measured value and independent of wavelength; they also need to assume extreme parameters for the stellar wind – a velocity of 50 km s^{-1} and a temperature of 10^6 K at 0.04 AU. With these assumptions, they reproduced the Lyα profile assuming an escape rate decreased with respect to previous models, to $\sim 10^9$ g s^{-1}.

4.2 Understanding the dynamics of an evaporating atmosphere

Numerical models of atmospheres enduring hydrodynamic escape were initially built to explain the loss of hydrogen from the primitive terrestrial and cytherean atmospheres (Watson, Donahue & Walker 1981; Kasting & Pollack 1983; Chassefière 1996). The discovery of HD 209458b evaporation sparked new modelling insights, which led to a better understanding of the dynamics subtending an energy-limited atmospheric escape. The evaporation was enhanced in the past, as the EUV stellar irradiation is more intense for young stars (Lammer et al. 2003; Penz, Micela & Lammer 2008). This irradiation is deposited across a large fraction of the extended atmosphere (Tian et al. 2005), which mainly cools via adiabatic expansion and radiative emissions from H_3^+, a product of molecular hydrogen photoionization (Yelle 2004, 2006). García-Muñoz (2007) provided one of the most exhaustive model of HD 209458b escaping atmosphere, including the effects of EUV heating, tidal forces (also treated in Lecavelier des Etangs et al. 2004), chemistry and ionization; this model is able to reproduce the observations of hydrogen, carbon, and oxygen.

[4]Roughly the same shape as an American football.

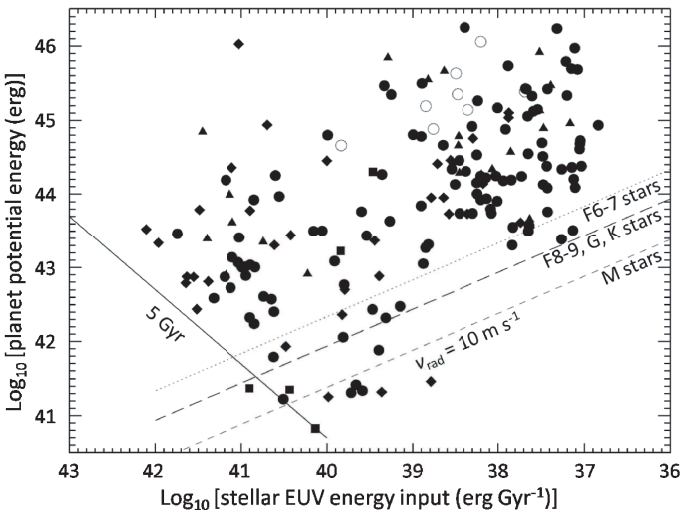

Fig. 4. Potential energy of exoplanets as a function of the mean EUV energy received per billion years. The different symbols represent planets around stellar types F (▲), G (●), K (♦), and M (■); a ○ denotes a class-III host star. The radial velocity detection limit of 10 m s^{-1} is plotted for different types of stars (dotted, dashed, and long-dashed lines). The masses and radii of non-transiting planets are taken to $\sqrt{2}m_p \sin i$ and inferred from mass-radius curves of Guillot (2005), respectively. After Lecavelier des Etangs (2007).

What all these detailed models basically agree on is that, despite some possible one-to-two-orders-of-magnitude variations around the canonical value of $\dot{m} \sim 10^{10}$ g s^{-1}, the atmosphere of HD 209458b – and probably of all massive hot Jupiters – is stable to hydrodynamic escape. This might not be the case, however, for lighter close-in exoplanets.

5 Atmospheric evaporation in the frame of comparative exoplanetology

Although a lot of detailed models has been developed to understand the physics of evaporation, it appears that the resulting escape rate does not depend on the details of the models but only on the assumed input energy used to escape the potential well of the planet. As a consequence, an energy diagram was introduced by Lecavelier des Etangs (2007) to evaluate the evaporation status of exoplanets.

It is represented in Fig. 4, and consists in plotting the potential energy one has to provide to a given planet in order to entirely escape its atmosphere, as a function of the EUV energy available from the star integrated through its life time. The ratio of these two quantities gives an estimate of the planet life time. The lack of planets in the lower right part of the diagram is a bias due to the precision of radial velocity measurements. While no observational bias prevents planets to be

found in the lower left-part of the diagram (at low separations), there is clearly a dearth of planet in this region. An enhanced evaporation could have make planets close to the 5-Gyr isochrone, such as 'hot-Neptunes' GJ 436b (23 Earth masses, $M_\oplus$) and GJ 581b (16 $M_\oplus$), or 'super-Earth' GJ 876d (7.5 $M_\oplus$), evolved away from the lower-left part of the diagram. These objects could be the remnants of planets initially 3, 4.5, and 13 times more massive, respectively. Evaporation should not have depleted GJ 436b from a hydrogen envelope (Gillon et al. 2007), hence it could still be evaporating today. Detecting its extended exosphere and measuring its escape rate would bring new constraints on the fate of close-in planets.

To test whether evaporation can alter a significant fraction of planets, Penz, Micela & Lammer (2008) estimated a distribution of stellar X-ray luminosity and its impact on various distributions of planetary initial masses. They showed that – not surprisingly – after 4 Gyr, 100% of HD 209458b-like planets would survive to atmospheric escape. Barely less (95%) would be wiped out if they were twice closer to the star. In the meantime, 80% of planets with an initial mass and density (2 g cm^{-3}) close to GJ 436b's would resist. Interestingly, less than 50% of lower-density hot-Neptunes ($\sim$ 1 g cm^{-3}) could survive evaporation, and 85% could be eroded down to super-Earth masses.

6 Summary

A planetary transit in the ultraviolet produces remarkably large spectroscopic signatures compared to what is observed in the visible. So far, the observational results obtained on planet HD 209458b have been obtained from two different instruments and strengthened by independent data analysis. The evaporation of close-in extrasolar planets also relies on a solid theoretical ground. Progress will come from the observations of other cases of extended exospheres and evaporation remnants. This will be feasible after *HST* Servicing Mission 4, which aims are – among other few – to fix STIS and install the Cosmic Origins Spectrograph (COS; Green, Wilkinson & Morse 2003).

The author warmly thanks A. Vidal-Madjar and A. Lecavelier des Etangs for their careful readings and useful inputs. He acknowledges support from the Agence Nationale de la Recherche through ANR grant NT05-4_44463.

References

Ben-Jaffel, L. 2007, ApJL, 671, L61

Bouchy, F., Udry, S., Mayor, M. et al. 2005, A&A, 444, L15

Chamberlain, J.W. & Hunten, D.M. 1987, *Theory of planetary atmospheres: an introduction to their physics and chemistry*, International Geophysics Series, 36 (Orlando: Academic Press, Inc.)

Charbonneau, D., Brown, T.M., Latham, D.W. & Mayor, M. 2000, ApJL, 529, L45

Charbonneau, D., Brown, T.M., Noyes, R.W. & Gilliland, R.L. 2002, ApJ, 568, 377

Chassefière, E. 1996, J. Geophys. Res., 101 (E11), 26039

Eggleton, P.P. 1983, ApJ, 268, 368
Ehrenreich, D., Lecavelier des Etangs, A., Hébrard, G. et al. 2008, A&A, 483, 933
Ford, H.C., Clampin, M., Hartig, G.F. et al. 2003, SPIE, 4854, 81
García Muñoz, A. 2007, P&SS, 55, 1426
Gillon, M., Demory, B.-O., Barman, T. et al. 2007, A&A 471, L51
Green, J.C., Wilkinson, E. & Morse, J.A. 2003, SPIE 4854, 72
Gu, Lin & Bodenheimer 2003, ApJ, 588, 509
Guillot, T. 2005, Annu. Rev. Earth Planet. Sci., 33, 493
Jeans, J.H. 1925, *The dynamical theory of gases* (Cambridge: University Press)
Kasting, J.F. & Pollack, J.B. 1983, Icarus, 53, 479
Hameury, J.-M. 2000, in *Étoiles doubles*, École CNRS de Goutelas, 23, 57, Egret, D., Halbwachs, J.-L. & Hameury, J.-M., editors
Henry, G.W., Marcy, G.W., Butler, R.P., Vogt, S.S. 2000, ApJL, 529, L41
Hunten, D.M. 1982, P&SS, 30, 773
Lammer, H., Selsis, F., Ribas, I. et al. 2003, ApJL, 598, L121
Lecavelier des Etangs, A., Vidal-Madjar, A., McConnell, J.C. & Hébrard, G. 2004, A&A, 418, L1
Lecavelier des Etangs, A. 2007, A&A, 461, 1185
Lecavelier des Etangs, A., Vidal-Madjar, A., Désert, J.-M. & Sing, D. K. 2008, A&A, in press (arXiv:0805.0595)
Moutou, C., Coustenis, A., Schneider, J. et al. 2001, A&A, 371, 260
Paczyński, B. 1971, ARA&A, 9, 183
Penz, T., Micela, G. & Lammer, H. 2008, A&A, 477, 309
Rauer, H., Bockelée-Morvan, D., Coustenis, A., Guillot, T. & Schneider, J. 2000, A&A, 355, 573
Sato, B., Fischer, D.A., Henry, G.W. et al. 2005, ApJ, 633, 465
Sing, D.K., Vidal-Madjar, A., Désert, J.-M., Lecavelier des Etangs, A. & Ballester, G. 2008, ApJ, in press (arXiv:0802.3864)
Smith, G.R. & Hunten, D.M. 1990, Rev. Geophys., 28, 117
Snellen, I.A.G., Albrecht, S., de Mooij, E.J.W., Le Poole, R.S. 2008, A&A, in press (arXiv:0805.0789)
Tian, F., Toon, O.B., Pavlov, A.A. & De Sterck, H. 2005, ApJ, 621, 1049
Vidal-Madjar, A. 1975, Solar Physics, 40, 69
Vidal-Madjar, A. 2005, in *Formation planétaire et exoplanètes*, École CNRS de Goutelas, 28, 243, Halbwachs, J.-L., Egret, D. & Hameury, J.-M., editors
Vidal-Madjar, A., Lecavelier des Etangs, A., Désert, J.-M. et al. 2003, Nature, 422, 133
Vidal-Madjar, A., Désert, J.-M., Lecavelier des Etangs, A. et al. 2004, ApJL, 604, L69
Vidal-Madjar, A., Lecavelier des Etangs, A. 2004, in *Extrasolar planets: today and tomorrow*, ASP Conf. Ser., 321, 152, Beaulieu, J.-P., Lecavelier des Etangs, A. & Terquem, C., editors
Vidal-Madjar, A., Lecavelier des Etangs, A., Désert, J.-M. et al. 2008, ApJL, 676, L57
Walker, J.C.G. 1982, Precambrian Research, 17, 147
Watson, Donahue & Walker 1981
Woodgate, B.E., Kimble, R.A., Bowers, C.W. et al. 1998, PASP, 110, 1183
Yelle, R.V. 2004, Icarus, 170, 167, and corrigendum (Yelle, R.V. 2006, Icarus, 183, 508)